Parallel and oblique proton fire hose instabilities in the presence of alpha/proton drift: Hybrid simulations

Petr Hellinger and Pavel Trávníček

Institute of Atmospheric Physics, AS CR, Prague, Czech Republic

Abstract. Parallel and oblique proton fire hose instabilities are investigated in the presence of a small abundance of alpha particles with a non zero drift velocity with respect to protons. Both instabilities scatter protons and alpha particles in the perpendicular direction with respect to the ambient magnetic field and decelerate both species with respect each other; especially the oblique fire hose effectively diffuses ions owing to its non quasi-linear evolution. Linear Vlasov theory predicts that the presence of the alpha/proton drift enhances the maximum growth rates of the two instabilities in a similar way and that the parallel fire hose is typically the dominant instability. On the other hand, the oblique fire hose has often the maximum growth rate comparable to that of the parallel one and hybrid simulations show that the oblique instability may be active even when the parallel one is marginally stable. Consequently, both instabilities are relevant in the solar wind context.

1. Introduction

A simple picture of the solar wind expanding in the radial magnetic field predicts a development of strong ion temperature anisotropies $T_{s\|} > T_{s\perp}$ (for symbol definitions see Appendix): Conservation of the two first adiabatic invariants [see, e.g., *Schulz and Eviatar*, 1973] naturally leads to such strong anisotropies. However, these invariants are broken when important collisions, heat fluxes or wave-particle interactions are present. Indeed, in situ observations show that the opposite anisotropy of the (core) solar wind protons $T_{p\|} < T_{p\perp}$, is common [*Kasper et al.*, 2003; *Marsch et al.*, 2004, and references therein]. This opposite anisotropy is probably a signature of dissipation processes of the solar wind turbulence [e.g. *Hollweg and Isenberg*, 2002, and references therein].

The properties of the solar wind ions are also determined by local plasma instabilities. For example, the proton cyclotron instability may reduce the proton temperature anisotropy in the case of $T_{p\|} < T_{p\perp}$ [*Gary et al.*, 2001]. On the other hand, in high β solar wind plasmas (i.e. for $\beta_p \gtrsim 1$) the (core) proton anisotropy $T_{p\|} > T_{p\perp}$ is often observed [*Kasper et al.*, 2002; *Marsch et al.*, 2004]. The linear theory of the bi-Maxwellian, homogeneous, proton-electron plasma predicts two instabilities driven by the proton temperature anisotropy $T_{p\|} > T_{p\perp}$: The right-handed (R-H) magnetosonic/whistler or electromagnetic ion cyclotron branch becomes unstable with a maximum growth rate at the parallel propagation – the parallel fire hose [*Quest and Shapiro*, 1996; *Farrugia et al.*, 1998; *Gary et al.*, 1998] whereas the left-handed (L-H) Alfvén or ion cyclotron branch changes the dispersion properties (gets non-propagating and almost linearly polarized) and become unstable at a strongly oblique propagation – the oblique fire hose [*Hellinger and Matsumoto*, 2000]. The threshold of the former instability is typically lower than that of the latter one in a bi-Maxwellian plasma. However, numerical simulations indicate that a plasma (marginally) stable with respect to the parallel fire hose may be unstable with respect to the oblique fire hose [*Hellinger and Matsumoto*, 2001].

The parallel fire hose is a resonant instability for $\beta_{p\|} \lesssim 25$ and the hybrid numerical simulations [*Gary et al.*, 1998] show that its non-linear evolution is essentially quasi-linear (at least for relatively modest growth rates): the unstable waves grow, saturate near the marginal stability and keep about the same amplitude with a little or none damping after the saturation. The anisotropic protons are slightly heated in the perpendicular direction. Hybrid expanding box simulations [*Hellinger et al.*, 2003; *Matteini et al.*, 2006] show that the parallel fire hose exhibits a marginal stability evolution analogous to the magnetosheath marginal stability with respect to the ion cyclotron waves [*Hellinger and Trávníček*, 2005].

The oblique fire hose is non-resonant and has a zero real frequency. Its saturation and non-linear evolution is very different from the quasilinear one: the waves generated by the instability undertake a strong branch/dispersion change and a large amount of the generated wave energy goes back to protons. This evolution makes the oblique fire hose more efficient in removing the proton temperature anisotropy than the parallel one. Hybrid expanding box simulations [*Hellinger et al.*, 2003] show that the oblique fire hose exhibits a different evolution from the marginal stability: the system oscillates between the stable and marginally stable regions.

The solar wind plasma contains small abundances of heavy ions. The most important heavy ions are alpha particles which have typically abundances around few percents of the electron number density [*Bame et al.*, 1975]. The presence of alpha particles changes plasma properties, for example, the growth rate of the parallel fire hose instability strongly depends on the alpha-particle abundance, (parallel) temperature and temperature anisotropy [and other plasma parameters, see *Dasso et al.*, 2003, and references therein].

Wind/SWE observations [*Kasper et al.*, 2002] indicate that there exists a constraint on the proton temperature anisotropy A_p which may be expressed in the form

$$A_p = \frac{T_{p\perp}}{T_{p\|}} \gtrsim 1 - \frac{a}{\beta_{p\|}^b} \quad (1)$$

with $a \sim 1$ and $b \sim 0.7$. This phenomenological constraint is compatible with the linear threshold condition for the parallel fire hose and with results of 1-D hybrid simulations [*Gary et al.*, 1998].

In situ observations in the fast solar wind [*Marsch et al.*, 1982; *Neugebauer et al.*, 1996; *Reisenfeld et al.*, 2001] show that alpha particles are typically faster than (core) protons and that the alpha/proton velocity $v_{\alpha p}$ (henceforth we will use "alpha/proton velocity" as a short-hand for "relative magnetic-field-aligned velocity between the two species") is comparable with the local Alfvén velocity. This is again in disagreement with the simple picture of the solar wind expanding in the radial magnetic field [cf. *Hellinger et al.*, 2003]. The alpha/proton velocity in the solar wind seems to be regulated through an interaction with solar wind waves and/or turbulence [e.g. *Hu and Habbal*, 1999; *Kaghashvili et al.*, 2003].

Many different instabilities likely constrain the alpha/proton velocity. The alpha/proton velocity itself is a source of free energy for

0148-0227/06/2005JA011318$9.00

beam-type instabilities, for instance the Alfvén and magnetosonic instabilities [e.g. *Montgomery et al.*, 1975; *Daughton and Gary*, 1998; *Gary et al.*, 2000; *Araneda et al.*, 2002]. The alpha/proton velocity is also regulated by instabilities driven by ion temperature anisotropies; in the case of $T_\perp > T_\parallel$ the alpha cyclotron and mirror instabilities decelerate the alpha particles (with respect to protons) whereas the proton cyclotron instability accelerate them [*Gary et al.*, 2003; *Hellinger and Trávníček*, 2005]. The proton distributions in the fast solar wind often contain two populations, a core and a tenuous beam propagating faster than the proton core. The proton/proton velocity (a short-hand for "relative magnetic-field-aligned velocity between the beam and core protons") is likely regulated in a similar way as in the case of the alpha/proton velocity [*Goldstein et al.*, 2000; *Kaghashvili et al.*, 2004]. The behavior of the alpha/proton and proton/proton velocity is not yet well understood [cf. *Tu et al.*, 2004]. In the present paper we investigate the two fire hose instabilities in the presence of a non-zero alpha/proton velocity.

This paper is organized as follows: First, in section 2 we investigate the linear theory of the two instabilities. Then in section 3 we present simulation results and, finally, in section 4 we discuss the simulation results and their implications in the solar wind context.

2. Linear Theory

The presence of alpha particles (with $v_{\alpha p} = 0$) does not qualitatively change the physical properties of the two fire hose instabilities. The growth rate of the parallel fire hose relatively strongly depends on the properties of alpha particles as well as on the (parallel) electron temperature and the electron temperature anisotropy [*Dasso et al.*, 2003]. It is interesting to note that a similar dependence is also observed in the case of the oblique fire hose. In this paper we extend the investigation of the parametric dependence, we include an additional parameter, the alpha/proton velocity $v_{\alpha p}$. When there is a non-zero $v_{\alpha p}$ the properties of R-H branch propagating parallel and anti-parallel with respect to $\boldsymbol{v}_{\alpha p}$ are different. The anti-parallel mode has larger growth rates than the parallel one; this is not true when the magnetosonic alpha/proton instability appears since it drives unstable only the parallel mode. Figure 1 demonstrates quantitatively this behavior: It displays a gray scale plot of the maximum growth rate of the R-H ion cyclotron waves as a function of the alpha/proton velocity $v_{\alpha p}$ and $\beta_{p\parallel}$ for $A_p = 0.4$ and $\beta_\alpha = 0.14$. The maximum growth rate is calculated for parallel waves with $k > 0$ and $\omega > 0$ and the sign of $v_{\alpha p}$ gives the parallel ($v_{\alpha p} > 0$) and anti-parallel ($v_{\alpha p} < 0$) propagation. Figure 1 clearly shows that the anti-parallel waves have larger growth rates than the parallel waves. The magnetosonic alpha/proton instability appears for $v_{\alpha p} \gtrsim 1.8$ at the parallel propagation. For $n_\alpha/n_e = 0.05$ and $\beta_\alpha = 0.14$ an approximate threshold value for the (anti-)parallel proton fire hose instability may be given as

$$A_p \propto 1 - \frac{a}{(\beta_{p\parallel} - \beta_0)^b} \tag{2}$$

where the fitting parameters a, b, and β_0 depend on $v_{\alpha p}$ as

$$\begin{aligned} a &\simeq 0.44 - 0.050|v_{\alpha p}|/v_A, \\ b &\simeq 0.50 + 0.042 v_{\alpha p}^2/v_A^2, \\ \beta_0 &\simeq 0.58 - 0.077|v_{\alpha p}|/v_A. \end{aligned}$$

This expression was obtained by fitting the relation for the maximum growth rate $\gamma(\beta_{p\parallel}, A_p, v_{\alpha p}) = 10^{-3}\omega_{cp}$ in the region $0.1 \le \beta_{p\parallel} \le 10$, $0.1 \le A_p \le 10$ and $|v_{\alpha p}| \le 2v_A$. It interesting to note that the $1/\beta_{p\parallel}^b$ dependence in equations (1,2) is valid for high beta plasmas $\beta_{p\parallel} > 1$ whereas the β_0 term becomes important for $\beta_{p\parallel} \lesssim 1$.

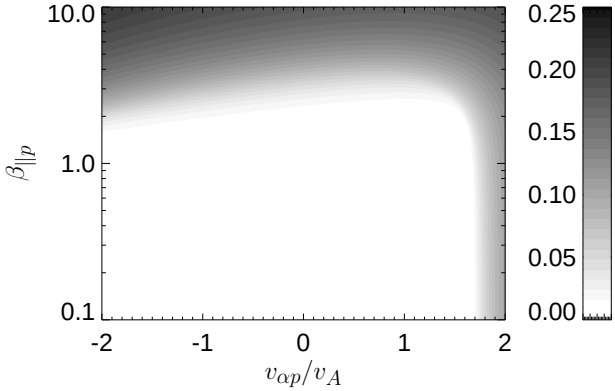

The gray scale is shown in units of ω_{cp} at the right panel.

Figure 1. Gray scale plot of the maximum growth rate of the R-H ion cyclotron branch as a function of the alpha/proton velocity $v_{\alpha p}$ and $\beta_{p\parallel}$.

The growth rate of the oblique fire hose also depends on $v_{\alpha p}$ as shown in Figure 2. Figure 2 shows maximum growth rates of the oblique fire hose, and of the parallel and anti-parallel fire hose (and of the magnetosonic alpha/proton instability) as a function of $|v_{\alpha p}|$ for $\beta_{p\parallel} = 2.52$, $A_p = 0.4$ and $\beta_\alpha = 0.14$: the solid curve denotes the maximum growth rate of the parallel fire hose propagating anti-parallel with respect to $\boldsymbol{v}_{\alpha p}$ (this branch corresponds to the negative values of $v_{\alpha p}$ in Figure 1), whereas the dashed curve denotes the maximum growth rate of the parallel fire hose (and the magnetosonic alpha/proton instability) propagating along to $\boldsymbol{v}_{\alpha p}$ (this branch corresponds to the positive values of $v_{\alpha p}$ in Figure 1). Stars denote the maximum growth rate of the oblique fire hose. It is interesting to note that the maximum growth rates of the parallel and oblique fire hoses are comparable and that they increase with $v_{\alpha p}$ in a similar manner.

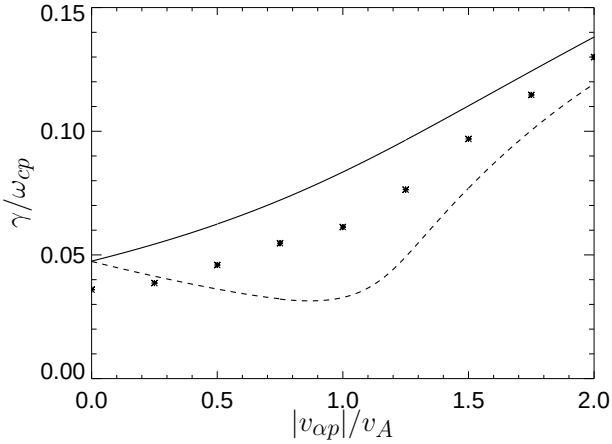

Figure 2. Maximum growth rates of the oblique fire hose, and of the parallel and anti-parallel R-H modes as a function of $|v_{\alpha p}|$ for $\beta_{p\parallel} = 2.52$, $A_p = 0.4$ and $\beta_\alpha = 0.14$. Solid and dashed curves correspond to negative and positive values of $\boldsymbol{v}_{\alpha p}$, respectively. Stars denote the maximum growth rate of the oblique fire hose.

Figure 3 shows the resonant factors ζ_p^+ and ζ_α^+ (see Appendix) of (solid) protons and (dashed) alpha particles, respectively, at the maximum growth rate as a function of the alpha/proton $v_{\alpha p}$. This

shows the characteristic properties of the parallel and anti-parallel instabilities: The anti-parallel fire hose is strongly resonant with protons ($|\zeta_p^+| \sim 2$) and it is less or non-resonant with alpha particles ($|\zeta_\alpha^+| \gtrsim 3$) whereas at the parallel propagation protons become less resonant ($|\zeta_p^+| \sim 2.5$ for $v_{\alpha p} > v_A$) and alpha particles become strongly resonant for the alpha/proton magnetosonic instability ($|\zeta_\alpha^+| \lesssim 1.5$ for $v_{\alpha p} > v_A$). On the other hand, the oblique fire hose is (cyclotron-wise) non-resonant with respect both to protons and alpha particles [cf. *Hellinger and Matsumoto*, 2000].

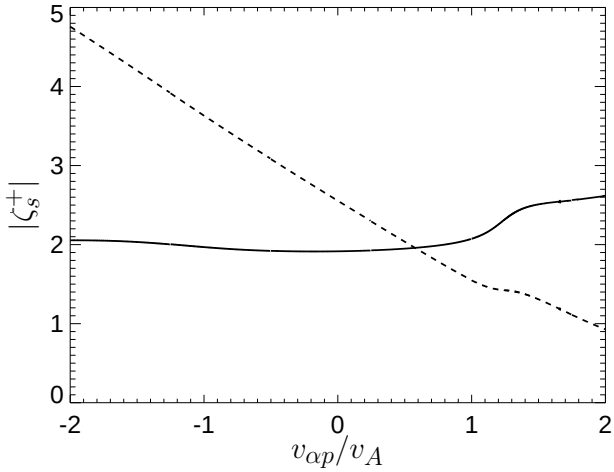

Figure 3. Resonant factors ζ_p^+ and ζ_α^+ of (solid) protons and (dashed) alpha particles, respectively, at the maximum growth rate for the (anti-)parallel fire hose (and for the magnetosonic alpha/proton instability) as a function of the alpha/proton velocity $v_{\alpha p}$ for $\beta_{p\|} = 2.52$, $A_p = 0.4$ and $\beta_\alpha = 0.14$.

The dispersion of the oblique fire hose in the case of $v_{\alpha p} \neq 0$ is different from the case of $v_{\alpha p} = 0$. The frequency of the oblique fire hose is not generally zero but it oscillates (as a function of k) around 0 with an amplitude equal to a small fraction of ω_{cp}. At the maximum growth rate these waves have a non-zero frequency and an oblique propagation angle $0^\circ < |\theta_{\boldsymbol{kB}}| < 90^\circ$ (note that we use $\theta_{\boldsymbol{kB}}$ in the range from -180° to 180°). The comparison of the growth rates and dispersion of the anti-parallel and oblique fire hoses is shown in Figure 4. Figure 4 displays the dispersion of the unstable waves, the frequency ω as a function of wave vector k for the anti-parallel ($\theta_{\boldsymbol{kB}} = 180^\circ$) R-H (upper gray-colored curve) and the oblique ($\theta_{\boldsymbol{kB}} = 56^\circ$) L-H branches (lower gray-colored curve). The gray colors encode the growth rate [cf. Plate 4 of *Hellinger and Matsumoto*, 2000]. The gray scale is shown in units of ω_{cp} at the right panel.

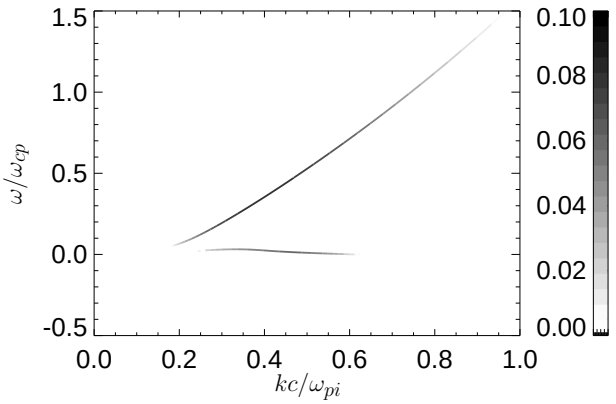

Figure 4. Dispersion of the unstable waves, the frequency ω as a function of wave vector k for the anti-parallel ($\theta_{\boldsymbol{kB}} = 180^\circ$) R-H (upper gray-colored curve) and the oblique ($\theta_{\boldsymbol{kB}} = 56^\circ$ L-H branches (lower gray-colored curve). The gray colors encode the growth rate. The gray scale is shown in units of ω_{cp} at the right panel.

3. Simulation Results

For numerical simulations we use a 2-D hybrid code developed by *Matthews* [1994]. In this code, electrons are considered as a massless, charge neutralizing fluid, with a constant temperature; ions are described by a particle-in-cell model and are advanced by a leapfrog scheme that requires the fields to be known at half time steps ahead of the particle velocities. This is achieved by advancing the current density to this time step with only one computational pass through the particle data at each time step. The particle contribution to the current density at the relevant mesh points is evaluated with bilinear weighting followed by smoothing over three points. No smoothing is performed on the electromagnetic fields, and the resistivity is set to zero in Ohm's law. The magnetic field is advanced in time with a modified midpoint method, which allows time substepping for the advance of the field.

We use following simulation parameters: The spatial resolution is $\Delta x = \Delta y = c/\omega_{pi}$, and there are 2048 and 1024 super-particles per cell for protons and alpha particles, respectively. The simulation box is in the x–y plane and is assumed to be periodic in both dimensions. Fields and moments are defined on a 2-D grid with dimensions $N_x \times N_y = 256 \times 256$. The time step for the particle advance is $\Delta t = 0.02/\omega_{cp}$ whereas the magnetic field $\boldsymbol{B}$ is advanced with a smaller time step, $\Delta t_B = dt/4$. The initial conditions are those investigated in the previous section in the frame of the linear Vlasov theory: the plasma is homogeneous in a homogeneous magnetic field $\boldsymbol{B}_0$ directed along the x axis, $\boldsymbol{B}_0 = (B_0, 0, 0)$, protons are anisotropic with $n_p/n_e = 0.9$, $\beta_{p\|} = 2.52$ and $A_p = 0.4$, alpha particles are isotropic, $A_\alpha = 1$, with $n_\alpha/n_e = 0.05$ and $\beta_\alpha = 0.14$. The simulation is performed in the frame where the ion current is zero, the proton and alpha velocities in this frame are field-aligned with $v_p = -0.1 v_A$ and $v_\alpha = 0.9 v_A$, respectively. The initial alpha/proton velocity is $v_{\alpha p} = v_A$. Finally, for electrons we set $\beta_e = 1$.

The evolution in the simulation may be divided into two phases. Each phase is dominated by a different instability. During the first phase the parallel fire hose appears and it saturates in a quasi-linear manner. Figure 5 shows the evolution of different quantities during the simulation: (a) the amplitude of the fluctuating magnetic field $|\delta\boldsymbol{B}|^2/B_0^2$, (b) the proton temperature anisotropy A_p, (c) the alpha/proton velocity $v_{\alpha p}$ (in units of v_A), and (d) the temperature

anisotropy of alpha particles A_α. During the initial growth protons and alpha particles are heated and decelerated with respect to each other. Generated waves interacts preferably with protons. From the second order theory [*Gary and Tokar*, 1985] one expects transport coefficients η_s for the ion velocities

$$\frac{\frac{dv_s}{dt}}{v_s} = \eta_s \frac{|\delta \boldsymbol{B}|^2}{B_0^2}. \quad (3)$$

The coefficient η_s is a collisionless (anomalous) equivalent to the classical collision frequency. In the simulation we observe $\eta_p \sim 0.32/\omega_{cp}$ and $\eta_\alpha \sim -0.072/\omega_{cp}$ (in a comparable 1-D simulation we have $\eta_p \sim 0.25/\omega_{cp}$ and $\eta_\alpha \sim -0.058/\omega_{cp}$). Similarly, the second order approximation predicts transport coefficients κ_s for the temperature anisotropies

$$\frac{\frac{dA_s}{dt}}{A_s} = \kappa_s \frac{|\delta \boldsymbol{B}|^2}{B_0^2}. \quad (4)$$

In the simulation we observe $\kappa_p \sim 0.73/\omega_{cp}$ and $\kappa_\alpha \sim 0.1$ (in a comparable 1-D simulation we have $\kappa_p \sim 0.60/\omega_{cp}$ and $\kappa_\alpha \sim 0.067$). Protons are scattered by the parallel fire hose more efficiently than alpha particles since protons are in a stronger cyclotron resonance with the waves than alpha particles (see previous section). The parallel fire hose saturates in a quasi-linear manner at $t \sim 80$; after the saturation, during the period $80 \lesssim t \lesssim 150$ the amplitude of the fluctuating magnetic field and other quantities are nearly constant.

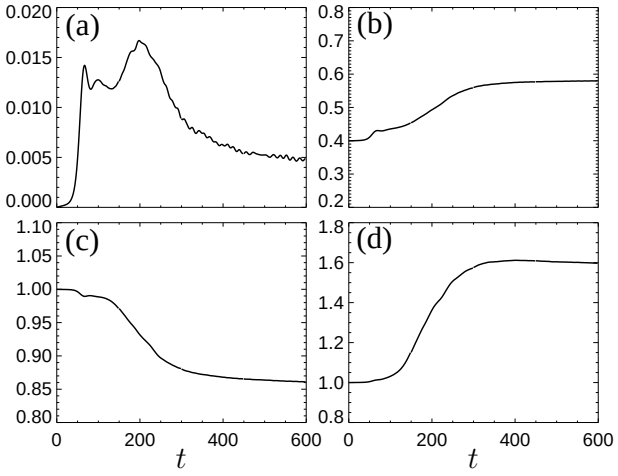

Figure 5. Evolution of different quantities: (a) the amplitude of the fluctuating magnetic field $|\delta \boldsymbol{B}|^2/B_0^2$, (b) the proton temperature anisotropy A_p, (c) the alpha/proton velocity $v_{\alpha p}$ (in units of v_A), and (d) the temperature anisotropy of alpha particles A_α.

The waves generated by the oblique fire hose grow during the first phase as well as those generated by the parallel one. The oblique waves continue to grow even after the saturation of the parallel fire hose and, during the second phase $t \gtrsim 150$, they reach important amplitudes. They are responsible for the peak of the magnitude of the fluctuating magnetic field at $t \sim 200$ (see Figure 5a) followed by a fast decrease. These oblique waves lead to a strong increase in A_p and A_α and to a decrease of $v_{\alpha p}$ which is more important than that resulting from the parallel fire hose. The appearance of the oblique fire hose disrupts the quasi-linear evolution of the parallel fire hose and it causes a disappearance of the waves generated by the parallel fire hose: This effect is demonstrated in Figure 6. Figure 6 shows the evolution of the amplitude of the fluctuating magnetic field $|\delta \boldsymbol{B}|^2/B_0^2$ as a function of time t and the propagation angle $\theta_{\boldsymbol{kB}}$. Figure 6 clearly shows the initial growth of the parallel fire hose waves at $\theta_{\boldsymbol{kB}} \sim 180^o$ (and at $\theta_{\boldsymbol{kB}} \sim 0^o$ with a smaller amplitude). The oblique fire hose appears at $|\theta_{\boldsymbol{kB}}| \sim 40^o$ later on. The oblique fire hose instability saturates via the dispersion change of the generated, almost linearly polarized waves (with $|\delta \boldsymbol{B} \times \boldsymbol{B}_0| \gg |\delta \boldsymbol{B} \cdot \boldsymbol{B}_0|$) to standard L-H waves at $|\theta_{\boldsymbol{kB}}| \sim 40^o$ and $|\theta_{\boldsymbol{kB}}| \sim 140^o$ [cf. *Hellinger and Matsumoto*, 2000]. The oblique wave activity is damped mainly via the cyclotron resonance with protons and alpha particles. At the end of the simulation there exist only waves at a quasi-parallel propagation. Ions heated by the oblique waves are no longer at the condition of the marginal stability with respect to the parallel waves and, consequently, these waves are suppressed.

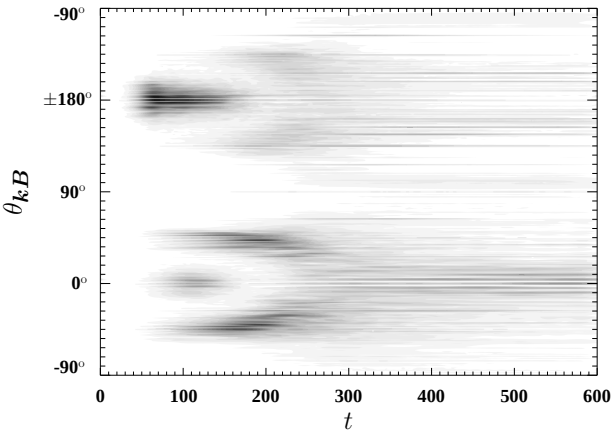

Figure 6. Amplitude of the fluctuating magnetic field $|\delta \boldsymbol{B}|^2/B_0^2$ as a function of time t and the propagation angle $\theta_{\boldsymbol{kB}}$.

Figure 7 gives a complementary view of the system evolution, it shows the amplitude of the fluctuating magnetic field $|\delta \boldsymbol{B}|^2/B_0^2$ as a function of time t and frequency ω; the spectrum was calculated using the wavelet transform of the time series of $\boldsymbol{B}$ at each grid point and averaged over all these grid points. Figure 7 shows the generation of the R-H waves during the first phase. It also displays the generation low-frequency waves (identified as the oblique ones, see Figure 6) and their damping during the second phase. At later times $t \gtrsim 300$ only the waves with $\omega \sim 0.1\omega_{cp}$ survive. These waves probably result from an inverse cascade towards longer wave lengths and quasi-parallel propagation [cf. *Hellinger and Matsumoto*, 2001].

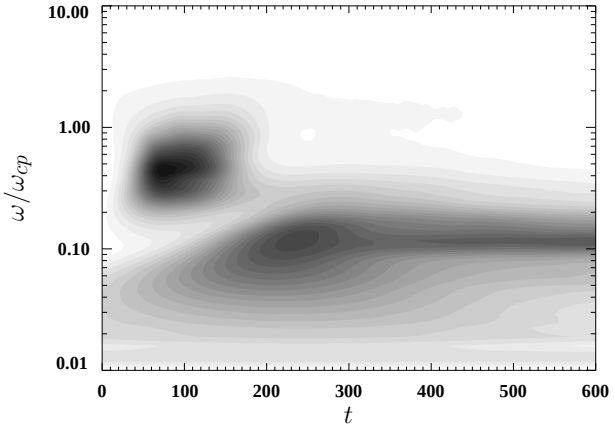

Figure 7. Amplitude of the fluctuating magnetic field $|\delta \boldsymbol{B}|^2/B_0^2$ as a function of time t and frequency ω (in units of ω_{cp}).

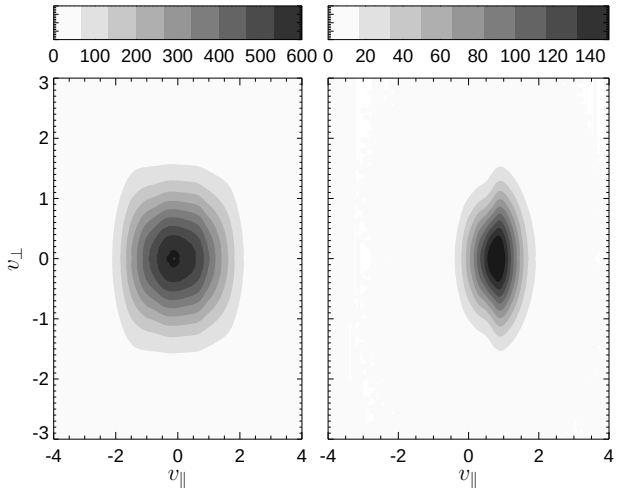

Figure 8. Gray scale plots of the reduced distribution functions (left) $f_p(v_\parallel, v_\perp)$ and (right) $f_\alpha(v_\parallel, v_\perp)$ at $t = 600/\omega_{cp}$. The gray scales are shown in arbitrary units at top panels. Velocities are given in units of v_A.

The waves generated by the two fire hose instabilities heat proton and alpha particles and slow both species with respect to each other. The wave-particle interactions lead to the development of strongly non Maxwellian distribution functions: Figure 8 shows gray scale plots of the proton and alpha reduced distribution functions (left) $f_p(v_\parallel, v_\perp)$ and (right) $f_\alpha(v_\parallel, v_\perp)$, respectively, at the end of the simulation ($t = 600/\omega_{cp}$). The complicated evolution of the simulated system affects mainly those particles with $|v_\parallel| \gtrsim v_A$; these particles exhibit signatures of the cyclotron resonance scattering [cf. *Marsch and Tu*, 2001]. The scattering of alpha particles is caused mainly by the cyclotron resonance with oblique waves resulting from the oblique fire hose instability. The scattering decelerates alpha particles and heats them in the perpendicular direction.

Distribution functions of the two species have also weak signatures of the Landau resonance. Figure 9 shows change in the distribution functions during the simulation, namely the difference $\Delta f_s(v_\parallel, v_\perp) = f_s(v_\parallel, v_\perp, t = 600/\omega_{cp}) - f(v_\parallel, v_\perp, t = 0/\omega_{cp})$ for (left) protons and (right) alpha particles. The gray scales are shown (in the same arbitrary units of Figure 8) at top panels. The dominant feature of the two Δf_s is the cyclotron diffusion of particles with initial velocities $|v_\parallel| \gtrsim v_A$ to higher $|v_\perp|$ (Figure 9, dark gray regions). Moreover, Δf_s exhibit constant $v_\parallel$ stripes for $|v_\parallel| \lesssim v_A$ which are likely signatures of the Landau resonance since the Landau diffusion does not depend on $v_\perp$ [cf. *Kennel and Engelmann*, 1966, Figure 2]. The changes in the distribution function due to the Landau resonance are however small compared to those generated by the cyclotron resonance since the generated oblique waves are transverse. Consequently, the dominant feature of the two ion distribution functions is the cyclotron diffusion of particles with initial velocities $|v_\parallel| \gtrsim v_A$ to higher $|v_\perp|$ Figure 8 (dark gray regions).

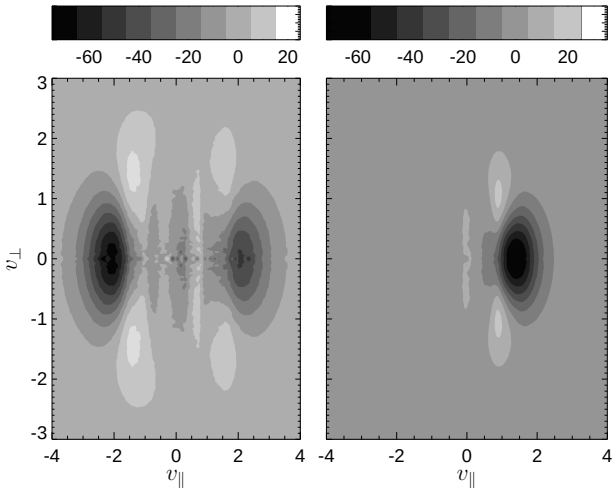

Figure 9. Gray scale plots of the changes of the reduced distribution functions $\Delta f_s = f_s(t = 600/\omega_{cp}) - f_s(t = 0/\omega_{cp})$ as functions of $v_\parallel$ and $v_\perp$ for (left) protons and (right) alpha particles during the simulation. The gray scales are shown (in the same arbitrary units of Figure 8) at top panels. Velocities are given in units of v_A.

4. Discussion and Conclusion

In the present paper we investigate linear and nonlinear properties of the proton parallel and oblique fire hose instabilities which appear for a sufficiently low value of A_p and a sufficiently high value of $\beta_{p\parallel}$. The maximum growth rate of the parallel fire hose relatively strongly depends on the properties of alpha particles as well as on the (parallel) electron temperature and the electron temperature anisotropy [*Dasso et al.*, 2003]. A similar dependence is also observed in the case of the oblique fire hose. Moreover, the linear Vlasov theory predicts that the alpha/proton velocity is another important factor which determines the growth rate of these two instabilities. The parallel fire hose is resonant with protons and less resonant with alpha particles whereas the oblique fire hose is non resonant. With a presence of a non-zero alpha/proton velocity the parallel instability becomes stronger at the anti-parallel propagation (compared to the parallel one) with respect to the alpha/proton velocity. For $n_\alpha/n_e = 0.05$ and $\beta_\alpha = 0.14$ the approximate constraint for the parallel proton fire hose instability may be given in the form of equation (2) similar to equation (1):

$$A_p \gtrsim 1 - \frac{a}{(\beta_{p\parallel} - \beta_0)^b}$$

where the fitting parameters a, b, and β_0 depend on $v_{\alpha p}$ as

$$\begin{aligned} a &\simeq 0.44 - 0.050|v_{\alpha p}|/v_A, \\ b &\simeq 0.50 + 0.042 v_{\alpha p}^2/v_A^2, \\ \beta_0 &\simeq 0.58 - 0.077|v_{\alpha p}|/v_A. \end{aligned}$$

For the parameters investigated in the present paper, the maximum growth rate of the (anti-)parallel fire hose increases with $v_{\alpha p}$. The maximum growth rate of the oblique instability is typically smaller than but comparable to that of the parallel one and exhibit a similar dependence on $v_{\alpha p}$.

A 2-D hybrid simulation reveals a complicated nonlinear evolution, a competition between the two instabilities [*Hellinger and*

Matsumoto, 2001]. The initial phase of the simulation is dominated by the parallel fire hose which saturates in the quasi-linear manner: The resulting scattering is moderate for protons and weak for alpha particles in agreement with its resonant properties. The oblique fire hose coexists with the parallel one and generates almost linearly polarized waves at a smaller growth rate. The oblique waves continue to grow even after the saturation of the parallel instability and saturate via a dispersion change of the linearly polarized waves to the standard L-H Alfvén (ion cyclotron) waves. These waves are strongly damped to ions via the cyclotron resonance; they also weakly interact with ions trough the Landau resonance. At the same time the parallel waves disappear as the oblique fire hose disrupts their marginal stability condition. Consequently, the oblique fire hose efficiently reduces the proton anisotropy and heats alpha particles and decelerates both species with respect each other.

In the hybrid code the electrons are treated as a massless, charge neutralizing fluid so that no electron kinetics is resolved. In particular, there is no Landau resonance of the oblique Alfvén waves with electrons. However, we expect that the electron Landau effect is weak in the present case: The simulation shows that the signatures of the proton Landau resonance are weak and the linear theory analysis by *Gary and Borovsky* [2004] indicates that for $\beta_e \sim 1$ and $\beta_p \sim 1$ the damping properties of the proton and electron Landau resonances are comparable. This expectation is clearly to be confirmed using a full particle code.

There are no observational evidences for the oblique fire hose instability to date. The phenomenological constraint [*Kasper et al.*, 2002], equation (1), is compatible with the threshold condition for the parallel fire hose instability. On the other hand, many observed proton anisotropies are relatively far from this constraint (and from the marginal stability). We suggest that these observations may be a consequence of the oblique instability.

In concluding, the parallel and oblique fire hose instabilities generated by the proton temperature anisotropy $T_{p\perp} < T_{p\parallel}$ are important mechanisms which reduce the proton temperature anisotropy and the alpha/proton velocity in the solar wind context. We expect that these instabilities may also reduce the proton/proton velocity in a similar way. These problems will be subject of future work.

Appendix: Glossary

$\perp$ and $\parallel$ denote the directions with respect to the ambient magnetic field $\boldsymbol{B}_0$, $B_0 = |\boldsymbol{B}_0|$ denotes its the magnitude while $\delta\boldsymbol{B}$ denotes the magnetic fluctuations. Subscript s denotes the ion specie (p stands for protons and α for alpha particles) or electrons (e). f_s denotes the velocity distribution function, and $T_{s\perp}$ and $T_{s\parallel}$ denote the perpendicular and parallel temperatures, respectively. T_s denotes the total temperature and A_s is the temperature anisotropy, $A_s = T_{s\perp}/T_{s\parallel}$. $\omega_{cs} = q_s B_0/m_s$ and $\omega_{ps} = (n_s q_s^2/m_s\epsilon_0)^{1/2}$ denote the cyclotron and plasma frequencies, respectively, $v_{s\parallel}$ and $v_{\mathrm{th}\parallel s}$ denote the mean parallel and the thermal velocity of the specie s, respectively. In these expressions m_s, q_s, and n_s denote the mass, the charge, and the number density (of the specie s), respectively, and ϵ_0 denotes the vacuum electric permittivity. $\beta_s = 2\mu_0 n_s k_B T_s/B_0^2$ and $\beta_{s\parallel} = 2\mu_0 n_s k_B T_{s\parallel}/B_0^2$ are the total and parallel betas, respectively; here μ_0 stands for the vacuum magnetic permeability and k_B is Boltzmann constant. $\boldsymbol{k}$, k, and $k_\parallel$ denote the wave vector, its magnitude and its parallel component. ω denotes a wave frequency. The resonant factors for parallel propagating wave with ω and $k = k_\parallel$ are given by

$$\zeta_s^{\pm} = (\omega - k v_{\parallel s} \pm \omega_{cs})/(\sqrt{2} k v_{\mathrm{th}\parallel s}). \qquad \text{(A1)}$$

The ion plasma frequency ω_{pi} is defined as $\omega_{pi} = (n_e e^2/m_p\epsilon_0)^{1/2}$ and the Alfvén velocity v_A is defined as $v_A = B_0/(\mu_0 n_e m_p)^{1/2}$.

Acknowledgments. Authors thank S. Peter Gary for useful discussions, and acknowledge the Czech grant GA AV IAA3042403 and ESA PECS No.98024.

Shadia Rifai Habbal thanks J. C. Kasper and Jaime Andres Araneda for their assistance in evaluating this paper.

References

Araneda, J. A., A. F. Viñas, and H. F. Astudillo (2002), Proton core temperature effects on the relative drift and anisotropy evolution of the ion beam instability in the fast solar wind, *J. Geophys. Res.*, 1453, doi: 10.1029/2002JA009337.

Bame, S. J., J. R. Asbridge, W. C. Feldman, and M. D. Montgomery (1975), Solar wind heavy ion abundances, *Solar Phys.*, *43*, 463–473.

Dasso, S., F. T. Gratton, and C. J. Farrugia (2003), A parametric study of the influence of ion and electron properties on the excitation of electromagnetic ion cyclotron waves in coronal mass ejections, *J. Geophys. Res.*, *108*, 1149, doi:10.1029/2002JA009558.

Daughton, W., and S. P. Gary (1998), Electromagnetic proton/proton instabilities in the solar wind, *J. Geophys. Res.*, *103*, 20,613–20,620.

Farrugia, C. J., F. T. Gratton, G. Gnavi, and K. W. Ogilvie (1998), On the possible excitation of electromagnetic ion cyclotron waves in solar ejecta, *J. Geophys. Res.*, *103*, 6543–6550.

Gary, S. P., and J. E. Borovsky (2004), Alfvén-cyclotron fluctuations: Linear Vlasov theory, *J. Geophys. Res.*, *109*, A06105, doi: 10.1029/2004JA010399.

Gary, S. P., and R. L. Tokar (1985), The second-order theory of electromagnetic hot ion beam instabilities, *J. Geophys. Res.*, *90*, 65–72.

Gary, S. P., H. Li, S. O'Rourke, and D. Winske (1998), Proton resonant firehose instability: Temperature anisotropy and fluctuating field constraints, *J. Geophys. Res.*, *103*, 14,567–14,574.

Gary, S. P., L. Yin, D. Winske, and D. B. Reisenfeld (2000), Alpha/proton magnetosonic instability in the solar wind, *J. Geophys. Res.*, *105*, 20,989–20,996.

Gary, S. P., R. M. Skoug, J. T. Steinberg, and C. W. Smith (2001), Proton temperature anisotropy constraint in the solar wind: ACE observations, *Geophys. Res. Lett.*, *28*, 2759–2763.

Gary, S. P., L. Yin, D. Winske, L. Ofman, B. E. Goldstein, and M. Neugebauer (2003), Consequences of proton and alpha anisotropies in the solar wind: Hybrid simulations, *J. Geophys. Res.*, *108*, 1068, doi: 10.1029/2002JA009654.

Goldstein, B. E., M. Neugebauer, L. D. Zhang, and S. P. Gary (2000), Observed constraint on proton-proton relative velocities in the solar wind, *Geophys. Res. Lett.*, *27*, 53–56.

Hellinger, P., and H. Matsumoto (2000), New kinetic instability: Oblique Alfvén fire hose, *J. Geophys. Res.*, *105*, 10,519–10,526.

Hellinger, P., and H. Matsumoto (2001), Nonlinear competition between the whistler and Alfvén fire hoses, *J. Geophys. Res.*, *106*, 13,215–13,218.

Hellinger, P., and P. Trávníček (2005), Magnetosheath compression: Role of characteristic compression time, alpha particle abundances and alpha/proton relative velocity, *J. Geophys. Res.*, *110*, A04210, doi: 10.1029/2004JA010687.

Hellinger, P., P. Trávníček, A. Mangeney, and R. Grappin (2003), Hybrid simulations of the expanding solar wind: Temperatures and drift velocities, *Geophys. Res. Lett.*, *30*, 1211, doi:10.1029/2002GL016409.

Hollweg, J. V., and P. A. Isenberg (2002), Generation of the fast solar wind: A review with emphasis on the resonant cyclotron interaction, *J. Geophys. Res.*, *107*, 1147, doi:10.1029/2001JA000270.

Hu, Y. Q., and S. R. Habbal (1999), Resonant acceleration and heating of solar wind ions by dispersive ion cyclotron waves, *J. Geophys. Res.*, *104*, 17,045–17,056.

Kaghashvili, E. K., B. J. Vasquez, and J. V. Hollweg (2003), Deceleration of streaming alpha particles interacting with waves and imbedded rotational discontinuities, *J. Geophys. Res.*, *108*, 1036, doi: 10.1029/2002JA009623.

Kaghashvili, E. K., B. J. Vasquez, G. P. Zank, and J. V. Hollweg (2004), Deceleration of relative streaming between proton components among nonlinear low-frequency Alfvén waves, *J. Geophys. Res.*, *109*, A12101, doi:10.1029/2004JA010382.

Kasper, J. C., A. J. Lazarus, and S. P. Gary (2002), Wind/SWE observations of firehose constraint on solar wind proton temperature anisotropy, *Geophys. Res. Lett.*, *29*, 1839, doi:10.1029/2002GL015128.

Kasper, J. C., A. J. Lazarus, S. P. Gary, and A. Szabo (2003), Solar wind temperature anisotropies, in *AIP Conf. Proc. 679: Solar Wind Ten*, edited by M. Velli, R. Bruno, and F. Malara, pp. 538–541, AIP, New York.

Kennel, C. F., and F. Engelmann (1966), Velocity space diffusion from weak plasma turbulence in a magnetic field, *Phys. Fluids*, *9*, 2377–2388.

Marsch, E., and C.-Y. Tu (2001), Evidence for pitch angle diffusion of solar wind protons in resonance with cyclotron waves, *J. Geophys. Res.*, *106*, 8357–8362.

Marsch, E., K. H. Muhlhauser, H. Rosenbauer, R. Schwenn, and F. M. Neubauer (1982), Solar-wind helium-ions – observations of the Helios solar probes between 0.3 AU and 1 AU, *J. Geophys. Res.*, *87*, 35–51.

Marsch, E., X.-Z. Ao, and C.-Y. Tu (2004), On the temperature anisotropy of the core part of the proton velocity distribution function in the solar wind, *J. Geophys. Res.*, *109*, A04102, doi:10.1029/2003JA010330.

Matteini, L., S. Landi, P. Hellinger, and M. Velli (2006), Parallel proton fire hose instability in the expanding solar wind: Hybrid simulations, *J. Geophys. Res.*, *111*, in preparation, doi:10.1029/2005JA.

Matthews, A. (1994), Current advance method and cyclic leapfrog for 2D multispecies hybrid plasma simulations, *J. Comput. Phys.*, *112*, 102–116.

Montgomery, M. D., S. P. Gary, D. W. Forslund, and W. C. Feldman (1975), Electromagnetic ion-beam instabilities in the solar wind, *Phys. Rev. Lett.*, *35*, 667–670.

Neugebauer, M., B. E. Goldstein, E. J. Smith, and W. C. Feldman (1996), Ulysses observations of differential alpha-proton streaming in the solar wind, *J. Geophys. Res.*, *101*, 17,047–17,056.

Quest, K. B., and V. D. Shapiro (1996), Evolution of the fire-hose instability: Linear theory and wave-wave coupling, *J. Geophys. Res.*, *101*, 24,457–24,469.

Reisenfeld, D. B., S. P. Gary, J. T. Gosling, J. T. Steinberg, D. J. McComas, B. E. Goldstein, and M. Neugebauer (2001), Helium energetics in the high-latitude solar wind: Ulysses observations, *J. Geophys. Res.*, *106*, 5693–5708.

Schulz, M., and A. Eviatar (1973), Validity of CGL equations in solar-wind problems, *J. Geophys. Res.*, *78*, 3948–3951.

Tu, C.-Y., E. Marsch, and Z.-R. Qin (2004), Dependence of the proton beam drift velocity on the proton core plasma beta in the solar wind, *J. Geophys. Res.*, *109*, A05101, doi:10.1029/2004JA010391.

P. Hellinger, P. Trávníček Institute of Atmospheric Physics, AS CR, Prague 14131, Czech Republic. (petr.hellinger@ufa.cas.cz; trav@ufa.cas.cz)